

Orthogonalized Kernel Regression for Spatial and Spatio-Temporal Residual Risk: Application to School Shootings in the Contiguous United States

Tilman M. Davies*

Department of Mathematics and Statistics, University of Otago

Michael R. Desjardins

Department of Epidemiology, Johns Hopkins Bloomberg School of Public Health

Alexander Hohl

Department of Geography, University of Utah

and

Guangzhen Wu

Department of Sociology & Criminology, University of Utah

June 1, 2026

Abstract

Distinguishing background heterogeneity from excess risk is a central challenge in case-control event data when both covariates and residual spatial or spatio-temporal structure matter. We develop a covariate-adjusted kernel regression framework that embeds an orthogonalized residual risk surface within a semiparametric binary model, and extend the approach from purely spatial to explicit spatio-temporal analysis. We apply the method to 959 gun violence incidents at public schools in the contiguous United States from 2000 to 2024, using incidents from the K-12 School Shooting Database linked to official school records for the corresponding year. The fitted models identify stable school-level associations, including markedly higher risk for larger schools and for middle and high schools, while also revealing substantial residual structure beyond the background distribution of schools. After adjustment for covariates, excess risk is found to remain concentrated in a persistent central-eastern corridor of the United States, with the strongest evidence appearing in recent years. More broadly, the analysis shows how residual risk surfaces can sharpen inference by separating background heterogeneity from anomalous structure in case-control event processes evolving over space and time.

*TMD acknowledges financial support from the Royal Society Te Apārangi (Marsden Fund Grant no. 23-UOO-148), and RSL/sabbatical funding from U. Otago.

Keywords: smoothing; point pattern; semiparametric model; gun violence

1 Introduction

Assessing the spatial distribution of events is a central problem in fields such as epidemiology, criminology, ecology, and public health (Gatrell et al. 1996, Velázquez et al. 2016, Bader 2025). When time-stamped records are available, interest often extends to how that spatial pattern evolves over time (González et al. 2016). In many applications, the main goal is not merely to map where events occur, but to identify locations at which their incidence is unusually high relative to an appropriate background population at risk (Bithell 1991). This distinction is important because the event pattern alone can be misleading: apparent ‘hotspots’, for instance, may simply reflect population heterogeneity.

Kernel-based relative-risk estimators provide a flexible way to make such comparisons. In the case-control setting, one estimates smooth spatial intensity or density surfaces for cases and controls and examines their ratio, yielding a continuously varying measure of relative risk over the study region (Kelsall & Diggle 1995, Davies et al. 2018). Analogous ideas have been extended to the spatio-temporal setting by smoothing jointly over space and time (Fernando & Hazelton 2014). These methods are attractive because they are visually interpretable, require relatively weak modeling assumptions, and permit direct identification of regions of relatively elevated or attenuated event incidence.

A key limitation of these techniques is that they do not readily accommodate point-level covariates, problematic in many applications where a portion of the apparent variation in risk may be explained by observed attributes of the individual events or entities under study. A solution was proposed by Kelsall & Diggle (1998), who embedded a kernel-based spatial relative-risk component within a generalized linear modeling framework. In their GAM-like construction, the smooth spatial component represents residual variation in event odds after adjustment for observed predictors. Although modern spatial and spatio-temporal generalized additive models are most often implemented using spline-based

smoothers, particularly thin-plate-type constructions (Wood 2017), kernel smoothers are particularly appealing when one wishes to preserve a localized relative-risk interpretation and straightforwardly obtain simulation-based summaries to, say, assess significance.

The present article extends kernel-based regression for case-control event data in two directions. Methodologically, we develop an orthogonalized fitting scheme that constrains the smooth residual term against the fixed-effects space, improving identifiability and helping separate covariate effects from residual spatial structure. Substantively, we extend the framework from the purely spatial setting to explicit spatio-temporal risk mapping, permitting continuous assessment of how residual risk evolves over both geography and time. These developments are motivated by a novel and sensitive application: shootings and gun-related violence at K-12 schools across the United States.

Recent empirical work has begun to use national school-shooting datasets, including the *K-12 School Shooting Database (SSDB)* (Riedman 2025), in more systematic ways. For example, Gammell et al. (2022) relate shooter, school, and incident characteristics to school-shooting severity; Fridel (2021) finds that school shootings are more likely in larger, more disadvantaged, and more violent district contexts; Joseph & Purser (2023) study how incident and perpetrator features relate to victim counts; and Wippell et al. (2026) examine school shootings at the state-year level as a function of firearm-law environments. However, this literature remains largely descriptive, incident-level, or geographically aggregated in focus. To our knowledge, the SSDB has not previously been used to support a continuous case-control spatial or spatio-temporal assessment of residual risk at the national scale. By linking SSDB incidents to contemporaneous school records from the National Center for Education Statistics, we show how covariate-adjusted residual risk surfaces can be estimated and interpreted for a problem of clear substantive importance.

The balance of the article is structured as follows. Section 2 describes the data, case linkage,

control selection, and predictors. Section 3 presents the models, fitting algorithms, and inferential summaries. Section 4 presents the results of the application, and we end with concluding remarks in Section 5.

2 Motivating Application

2.1 Background

Although by no means exclusive to the United States, gun-related violence at schools is an especially prominent concern in a country with exceptionally high rates of firearm violence relative to other high-income nations (Richardson & Hemenway 2011). The issue is highly complex, with social, epidemiological, demographic, and political dimensions (Rowhani-Rahbar & Moe 2019, Kolbe 2020, Stewart et al. 2022). Moreover, the public understanding of school gun violence is often shaped by a small number of highly publicized mass-casualty events, even though the broader landscape includes many incidents of differing severity, motivation, and circumstance (Kolbe 2020, Riedman 2025).

At the national level, school firearm incident data in the United States are not generated through a single unified official reporting system. Rather, available statistics are assembled from sources with differing scopes, definitions, and collection strategies, including both federal surveillance products and independent compilations (Stewart et al. 2022, Nowicki 2020). This fragmentation reflects, in part, the difficulty of defining what should count as a school gun violence event (Comer 2024, Riedman 2025). While some cases are unambiguous (e.g. multiple shots fired or multiple casualties), others are less clear. Brandishing, though not discharging, a firearm during a dispute on school grounds is one such example: no immediate physical injury may occur, yet the nature of the threat and its potential consequences may still justify inclusion.

These issues complicate efforts to obtain a macro-level nationwide understanding of school gun violence. Existing work often focuses on individual events or on descriptive summaries over relatively coarse spatial units (see for example the papers referenced in Section 1). As a result, comparatively little is known about how the risk of school gun violence events varies across the country after accounting for the background distribution of schools, school-level characteristics, and possible temporal change. Are apparent concentrations of incidents simply a reflection of where schools are located? Do school-level variables such as enrollment size and demographic composition explain some of the observed variation? How, if at all, has the residual geography of risk changed over time? Addressing such questions requires both suitable data and statistical tools capable of separating background heterogeneity driven by observed factors from genuinely anomalous risk. These issues motivate the present work.

2.2 Case Selection and NCES Linking

Our incident data are drawn from the aforementioned K-12 School Shooting Database (Riedman 2025), from which we extract qualifying firearm-related incidents at K-12 schools across the United States. Details of the SSDB’s data collection and verification procedures are available at <https://k12ssdb.org>. The SSDB contains a multitude of variables related to each recorded incident which we use to filter the raw data. We scrutinize the 25 years covering January 1st, 2000 through December 31st, 2024; these comprise 2,247 events. Although we take a fairly broad stance, our interest lies in those involving school students and/or staff on school property in which there was intent by the perpetrator to harm one or more individuals other than themselves, in either a premeditated or spontaneous fashion. This excludes those events deemed accidental or those in which an isolated suicide attempt was made; we also exclude those events with a low reliability indicator, meaning the incident must have been the subject of at least one news article with a named author. This initial

filtering exercise left 1,176 qualifying records.

In addition to incident date, time, school name, and city/state, the SSDB variables include school level, which we simplify to four categories: Primary/Elementary, Middle/Junior High, High/Senior High and Other (the latter reserved for a few dozen schools that could not easily be classified as per the preceding categories). Incident locations are provided as longitude/latitude decimal degrees; these WGS84 geographic coordinates (EPSG:4326) are projected via the NAD83 / Conus Albers Equal Area system (EPSG:5070) to planar coordinates in meters, before being rescaled to kilometers (km).

Though comprehensive in terms of the incidents themselves, general details on the schools associated with each event are limited to the aforementioned variables. To account for any additional covariates in modeling, like those related to school size or enrollment, it is necessary to match each incident school with official data made available by the National Center for Education Statistics (NCES), part of the Department of Education. The NCES allows the generation of data tables via the Elementary/Secondary Information System (EISi), wherein each school possesses a unique 12-digit ID along with a swath of descriptive information, including enrollment data. The database is indexed by school year, permitting a contemporary inspection of, say, the total enrollment count for any given year.

Owing to the fact the SSDB entries do not contain the NCES IDs, we implement a matching strategy to link each SSDB incident to a unique NCES school record for the corresponding year of the event using deterministic identifiers so that contemporaneous school data may be extracted from their government records. This is done by attempting to match on school name, broad location (state and city), and then confirming with school level, ZIP, and WGS84 coordinates; the exercise was complicated in part by the lack of a standardized naming scheme for schools in both the SSDB and the NCES datasets, as well as sporadic data entry errors in both. Following this matching exercise, we culled any schools associated

with level disagreements, nonsensical enrollment figures (e.g. zero enrolled students), or erroneous geographical coordinates. Furthermore, the decision was made to omit private schools from consideration here, given the official data is less complete for these institutions; ELSi ceased hosting data on private schools altogether after 2021.

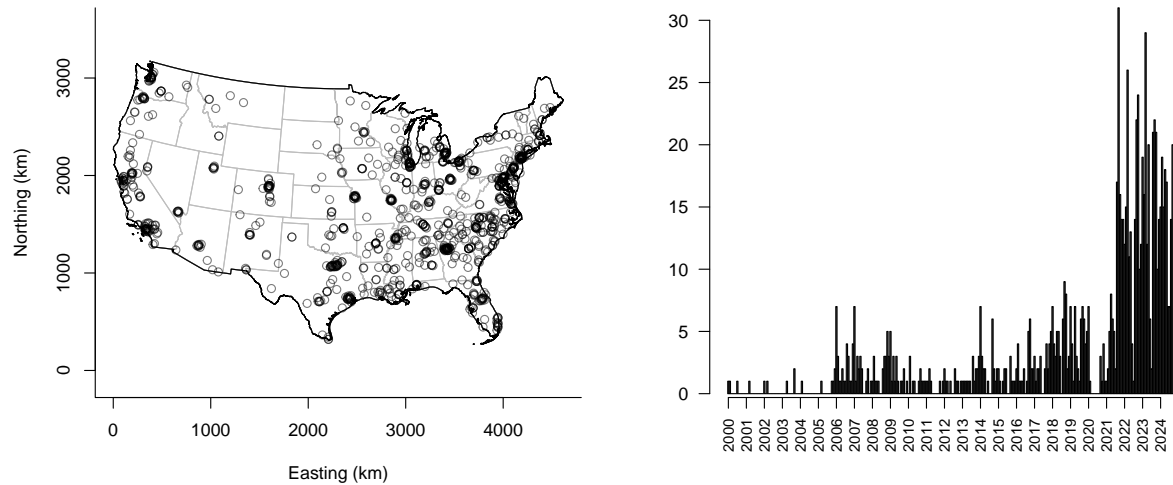


Figure 1: Spatial and temporal margins of 959 non-accidental gun violence events at public K-12 schools, 01/01/2000 - 12/31/2024.

The culmination of these efforts produced the final set of 959 NCES-matched school gun violence incidents between 01/01/2000 and 12/31/2024, and it is these cases which are used in all analyses and results in the remainder of this work. Their spatial and temporal margins are shown in Figure 1. Spatially, the case concentrations closely resemble the spatial distribution of K-12 schools across the continental 48 states (seen in the following section). Temporally, we note these incidents begin to occur more frequently from around 2006, with a dramatic increase following 2021 (a lull in 2020—almost certainly due to pandemic-related disruptions—also being visible).

2.3 Control Selection

Control points, used to adjust for the background heterogeneity of schools across the country, are drawn from the full set of NCES records restricted to the 48 contiguous states and the corresponding 25-year interval spanning the case data (2000-2024). Following removal of fully virtual schools, as well as those records with apparently incorrect or internally inconsistent enrollment numbers, the raw pool of potential controls forms 2,089,903 records. Note this comprises a combined stack of annual data; most individual schools therefore exist as multiple records in the pooled data set, allowing for contemporaneous snapshots of a given school’s enrollment and demographic descriptors over time.

For the analyses we draw a total of $c = 10$ controls per case—a pragmatic trade-off between estimate stability and computational burden—frequency-matched by calendar year to the case set. Concretely, if year t contains $n^{(t)}$ incidents, we sample without replacement $cn^{(t)}$ control school-year records from the NCES pool for that same year (after excluding any NCES IDs that appear among the cases). The models described in Section 3 use this pooled-by-year frequency matching. This ensures that, within each year, the case-control comparison is anchored to the school population as recorded in that same year, and avoids implicitly borrowing controls from years in which the national composition and size of the school population may differ. Temporal changes in overall incident prevalence are thus intentionally absorbed by the design of the case-control sample, allowing the modeling focus to remain on spatial pattern and magnitude of relative risk.

Rather than rely on a single generated set of controls, our final results are aggregated over multiple independent, identically sampled control sets (a “bagging” strategy). This provides a simple and effective way to reduce sensitivity to the particular random draw of controls and to stabilize the fitted risk surfaces and associated exceedance summaries.

A rotatable three-dimensional plot of the case data, along with a randomly generated year-

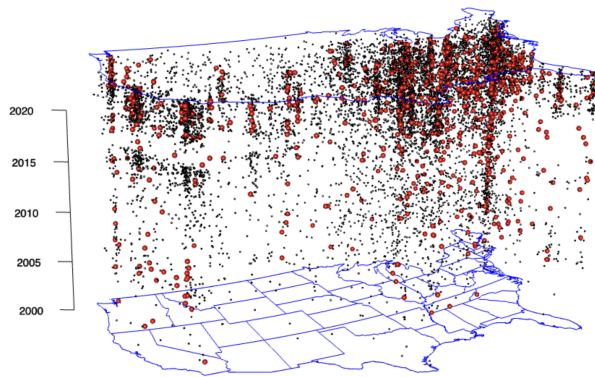


Figure 2: Spatio-temporal plot of the gun violence incidents (large/red points) alongside a random control draw of controls from the NCES/EI Si pool (small/black points); the latter is frequency-matched by incident year at a ratio of 10:1.

matched set of controls, is given in Figure 2. Here, the exact day-month-year timestamp is used for the cases, and the controls are uniformly scattered over the days of the year to which each belongs. The HTML file containing the interactive graphic is included in the supplement and is also accessible at <https://www.stats.otago.ac.nz/research/davies-gv/data.html>. As expected, the concentrations of gun violence incidents closely mimic the distribution of schools across the country—and it remains to be seen whether the incident risk is structured beyond the school-level covariates and the spatio-temporal distribution of the controls.

2.4 Predictor Variables

It is reasonable to expect that the occurrence of a gun violence event may be partially attributable to certain school-specific characteristics. For instance, a large school with many hundreds of students may be at higher risk than a much smaller (yet otherwise similar) school with only dozens of students, purely by virtue of size (Fridel 2021).

From the NCES records of each case and control, we retrieve (for the corresponding year) the total number of students, alongside the proportion of male students and the proportion of white students as coarse demographic composition measures, and combine these with

school level (Primary/Middle/High/Other). Additionally, we include a deprivation measure as a coarse proxy for broader socioeconomic context that is not captured by the NCES school descriptors. We extract the Area Deprivation Index (ADI) at the census-tract level from US Census/ACS-derived inputs (higher ADI indicating greater deprivation), and assign each case/control school-year record the ADI value corresponding to its location. Because tract-level ADI is not available annually over our full study period, we treat deprivation as time-invariant: each location is assigned a single tract-level ADI value taken as its average over the available years, and this value is carried across all school-years. Accordingly, the ADI coefficient should be interpreted as an association with a fixed location-level deprivation proxy rather than a within-tract temporal effect.

Although ADI is piecewise constant over census tracts rather than spatially continuous, we consider this discretization sufficiently fine relative to the national scale of the analysis. More generally, area-level covariates require care in interpretation vis-à-vis the “ecological fallacy”: effects reflect associations at the level at which the covariate is measured. For this reason we avoid including county- or state-level variables as predictors, since these operate at spatial scales substantially larger than the school-year observational unit and would raise sharper issues of spatial misalignment and interpretation. Broad spatial or spatio-temporal structure is instead represented through the residual surface component of the model.

3 Models, Implementation

We consider a semiparametric binary regression framework in which a fixed-effects component is combined with a kernel-smoothed residual risk field. The goal is to separate variation in case odds explained by observed covariates from residual spatial or spatio-temporal concentration. We achieve this using an orthogonalized iteratively reweighted least squares (o-IRLS) fitting scheme that embeds a Nadaraya-Watson smoother within the logistic

mean structure while constraining the residual smooth against the fixed-effects space. This preserves the interpretation of the smooth term as residual risk rather than allowing it to compete with the parametric component. We first describe a purely spatial model in detail, then extend the same construction to an explicit spatio-temporal setting. A grouped-time intermediate variant—interpretable as a bridging step between the two models presented here—was also explored, but is omitted from the main text for brevity and reported in the supplementary materials.

In what follows, we assume $n = n_0 + n_1$ observations, for which $y_i \in \{0, 1\}$ identifies the i th component as one of the n_0 controls ($y_i = 0$) or as one of the n_1 cases ($y_i = 1$); $i = 1, \dots, n$. We use $\mathbf{x}_i \in \mathbb{R}^{p+1}$ to denote the $(p + 1) \times 1$ vector of p predictor values, along with a baseline intercept term, for the i th entity; the full $n \times (p + 1)$ design matrix is given by $\mathbf{X} = [\mathbf{x}_1, \dots, \mathbf{x}_n]^\top$. Let $\mathbf{s}_i \in \mathcal{W} \subset \mathbb{R}^2$ be the corresponding planar coordinate of i .

3.1 Spatial Model

3.1.1 Definition

With $p_i = \Pr(y_i = 1 \mid \mathbf{x}_i, \mathbf{s}_i)$, consider

$$\text{logit } p_i = \mathbf{x}_i^\top \boldsymbol{\beta} + g(\mathbf{s}_i), \quad (1)$$

where $\boldsymbol{\beta} = [\beta_0, \dots, \beta_p]^\top$ is the $(p + 1) \times 1$ vector of regression coefficients and $g : \mathcal{W} \rightarrow \mathbb{R}$ is a smooth spatial function. The form of $g(\mathbf{s})$ is motivated by classical kernel methods for case-control relative-risk estimation ([Bithell 1991](#), [Kelsall & Diggle 1995](#), [Davies et al. 2018](#)).

Let $f_1(\mathbf{s})$ and $f_0(\mathbf{s})$ denote the spatial densities of case and control locations, respectively.

A natural measure of excess case incidence is the density ratio

$$r(\mathbf{s}) = \frac{f_1(\mathbf{s})}{f_0(\mathbf{s})}, \quad (2)$$

or, on the logarithmic scale, $\log r(\mathbf{s}) = \log f_1(\mathbf{s}) - \log f_0(\mathbf{s})$. Positive values of $\log r(\mathbf{s})$ indicate locations at which cases are relatively more concentrated than controls, while negative values indicate comparatively lower concentration.

This model retains this local case-control comparison while allowing adjustment for measured school-level covariates. Specifically, for fixed $\boldsymbol{\beta}$, define $g(\mathbf{s})$ at each location $\mathbf{s} \in \mathcal{W}$ as the value satisfying the kernel-weighted local score equation

$$\sum_{i=1}^n \kappa_h(\|\mathbf{s} - \mathbf{s}_i\|) \left[y_i - \text{logit}^{-1}\{\mathbf{x}_i^\top \boldsymbol{\beta} + g(\mathbf{s})\} \right] = 0, \quad (3)$$

where $\kappa_h(\mathbf{s}) = h^{-2} \kappa(h^{-1} \mathbf{s})$ is a radially symmetric spatial kernel ($\kappa : \mathbb{R}^2 \rightarrow \mathbb{R}$) with scalar bandwidth h . Thus, $g(\mathbf{s})$ is defined through a local kernel comparison of cases and controls after adjustment for the linear predictor $\mathbf{x}_i^\top \boldsymbol{\beta}$.

The link with the classical density-ratio construction (2) is clearest in the intercept-only case, where (3) becomes

$$\sum_{i=1}^n \kappa_h(\|\mathbf{s} - \mathbf{s}_i\|) \left[y_i - \text{logit}^{-1}\{\beta_0 + g(\mathbf{s})\} \right] = 0,$$

and solving this for the local fitted odds gives

$$\exp\{\beta_0 + g(\mathbf{s})\} = \frac{\sum_{i:y_i=1} \kappa_h(\|\mathbf{s} - \mathbf{s}_i\|)}{\sum_{i:y_i=0} \kappa_h(\|\mathbf{s} - \mathbf{s}_i\|)}.$$

Thus $\beta_0 + g(\mathbf{s})$ is the logarithm of the ratio of kernel-weighted case mass to kernel-weighted control mass. If this is expressed in terms of kernel intensity estimators, then $\beta_0 + g(\mathbf{s}) = \log\{\hat{\lambda}_1(\mathbf{s})/\hat{\lambda}_0(\mathbf{s})\}$. Alternatively, if $\hat{f}_1(\mathbf{s})$ and $\hat{f}_0(\mathbf{s})$ denote kernel density estimators for the case and control locations, then $\beta_0 + g(\mathbf{s}) = \log\{\hat{f}_1(\mathbf{s})/\hat{f}_0(\mathbf{s})\} + \log(n_1/n_0)$, so that the difference between these two formulations is absorbed into the intercept.

Although the representation $\text{logit } p_i = \mathbf{x}_i^\top \boldsymbol{\beta} + g(\mathbf{s}_i)$ resembles that of a spatial generalized additive model, the above shows the present construction is different in both motivation and estimation: $g(\mathbf{s})$ is defined through a kernel-localized case-control comparison rather

than through a generic basis-penalty smooth. In the following subsection, we show how a first-order IRLS linearization of (3) leads naturally to a Nadaraya-Watson kernel regression smoother of the working residuals, forming the basis of the fitting algorithm used here.

3.1.2 Implementation

We propose an orthogonalized iteratively reweighted least squares (o-IRLS) scheme for fitting. At a current iterate $(\boldsymbol{\beta}, \mathbf{g})$, where $\mathbf{g} = [g(\mathbf{s}_1), \dots, g(\mathbf{s}_n)]^\top$, define

$$\eta_i = \mathbf{x}_i^\top \boldsymbol{\beta} + g(\mathbf{s}_i), \quad p_i = \text{logit}^{-1}(\eta_i), \quad w_i = p_i(1 - p_i), \quad (4)$$

and form the usual working response

$$z_i = \eta_i + \frac{y_i - p_i}{w_i}. \quad (5)$$

With $\boldsymbol{\beta}$ held fixed, let

$$u_i = z_i - \mathbf{x}_i^\top \boldsymbol{\beta} \quad (6)$$

denote the partial residual.

Under the quadratic IRLS surrogate, updating $g(\mathbf{s})$ at a fixed location \mathbf{s} amounts to minimizing $\sum_{i=1}^n \kappa_h(\|\mathbf{s} - \mathbf{s}_i\|) w_i \{u_i - c\}^2$ over a local constant c . The minimizer is the Nadaraya-Watson kernel regression smoother applied to $\{u_i\}$, giving the provisional spatial field

$$\tilde{g}(\mathbf{s}|h) = \frac{\sum_{i=1}^n \kappa_h(\|\mathbf{s} - \mathbf{s}_i\|) w_i u_i}{\sum_{i=1}^n \kappa_h(\|\mathbf{s} - \mathbf{s}_i\|) w_i}. \quad (7)$$

Writing $\tilde{\mathbf{g}} = [\tilde{g}(\mathbf{s}_1|h), \dots, \tilde{g}(\mathbf{s}_n|h)]^\top$ and $\mathbf{W} = \text{diag}(w_1, \dots, w_n)$, we then enforce weighted orthogonality of the smooth term to the fixed-effects space by setting

$$\mathbf{g} = \tilde{\mathbf{g}} - \mathbf{X}(\mathbf{X}^\top \mathbf{W} \mathbf{X})^{-1} \mathbf{X}^\top \mathbf{W} \tilde{\mathbf{g}}. \quad (8)$$

This ensures $\mathbf{X}^\top \mathbf{W} \mathbf{g} = \mathbf{0}$, so the residual spatial field cannot absorb variation already attributable to the columns of \mathbf{X} . Given \mathbf{g} , the regression coefficients are updated by

weighted least squares:

$$\boldsymbol{\beta} \leftarrow (\mathbf{X}^\top \mathbf{W} \mathbf{X})^{-1} \mathbf{X}^\top \mathbf{W} (\mathbf{z} - \mathbf{g}), \quad (9)$$

where $\mathbf{z} = [z_1, \dots, z_n]^\top$. From a starting position of $\mathbf{g} = \mathbf{0}$ and $\boldsymbol{\beta} = \boldsymbol{\beta}^{(0)}$, where $\boldsymbol{\beta}^{(0)}$ are the regression coefficients from a standard logistic regression fit to the data, the o-IRLS loop (4)-(9) is repeated until convergence.

The orthogonalization step (8) is the key distinction from the IRLS algorithm of [Kelsall & Diggle \(1998\)](#). It is closely related in spirit to the restricted spatial regression idea of [Hodges & Reich \(2010\)](#): under the current IRLS weights, we remove from the provisional smooth any component lying in the weighted fixed-effects space. This keeps $g(\mathbf{s})$ interpretable as a residual risk surface while preserving the usual interpretation of the fixed-effects component. A further consequence of (8) is that, under frozen IRLS weights, the additive weighted least-squares subproblem is resolved by a one-step projection update rather than by an inner backfitting loop. This again differs from [Kelsall & Diggle \(1998\)](#), where smoothing and regression updates are alternated to convergence within each IRLS cycle.

3.1.3 Bandwidth Selection

The fitting scheme above assumes a fixed spatial bandwidth h in calculation of the provisional smooth. In practice, we select h by likelihood cross-validation. With fitted probabilities p_i and Fisher weights $w_i = p_i(1 - p_i)$, let $\tilde{g}^{[-i]}(\mathbf{s}_i|h^*)$ denote the leave-one-out kernel smooth at the i th site of the current partial residual field obtained under candidate bandwidth h^* .

Define

$$\eta_{i,h^*}^{[-i]} = \mathbf{x}_i^\top \boldsymbol{\beta} + \tilde{g}^{[-i]}(\mathbf{s}_i|h^*), \quad p_{i,h^*}^{[-i]} = \text{logit}^{-1}(\eta_{i,h^*}^{[-i]}).$$

The Bernoulli likelihood CV score is then

$$\text{CV}(h^*) = \sum_{i=1}^n \left[y_i \log p_{i,h^*}^{[-i]} + (1 - y_i) \log(1 - p_{i,h^*}^{[-i]}) \right], \quad (10)$$

with the leave-one-out construction preventing an interpolating solution. We select h as the maximizer of (10) over a candidate grid and insert it into the o-IRLS algorithm immediately prior to evaluation of (7). To reduce computation and stabilize the fit, this search is performed only during the first few IRLS updates, after which the selected value is held fixed. In fitting to the school gun violence data, the optimal bandwidth stabilized rapidly, typically within 5 or 6 iterations.

3.1.4 Inference and Assessment

Post-fit, inference focuses on the residual spatial field evaluated over a fine grid covering the study window. The fitted surface $\hat{g}(\mathbf{s})$ is obtained by applying the same kernel smoother used in the fitting algorithm to the final working residual field, now evaluated at grid locations. We also consider its exponentiated form $\exp\{\hat{g}(\mathbf{s})\}$, interpretable as a residual odds-ratio surface relative to the covariate-adjusted baseline.

To assess whether apparent residual structure exceeds that expected under a covariate-only explanation, we use a Monte Carlo reassignment scheme. We first fit the logistic model containing only the fixed-effects component $\mathbf{X}\boldsymbol{\beta}$, then use the fitted probabilities to generate replicated case-control labelings with the same total number of cases as observed. For each replicate dataset, the spatial model is refitted at the same fixed bandwidth h , and the resulting residual surface is evaluated on the same grid.

Let $\hat{g}^{(1)}(\mathbf{s}), \dots, \hat{g}^{(B)}(\mathbf{s})$ denote the residual surfaces from the B Monte Carlo replicates. At each grid location \mathbf{s} , we compute the exceedance probability

$$\hat{p}_+(\mathbf{s}) = \frac{1}{B} \sum_{b=1}^B I\{\hat{g}^{(b)}(\mathbf{s}) < \hat{g}(\mathbf{s})\}, \quad (11)$$

with an analogous lower-tail quantity obtained by reversing the inequality. Large values of $\hat{p}_+(\mathbf{s})$ therefore indicate locations at which the observed fitted surface exceeds most of its null replicates. Contours of these exceedance-probability surfaces provide a convenient

summary of unusually elevated residual risk.

A further source of variability arises from the random sampling of controls from the eligible school population. To assess stability with respect to this design step, we repeat the full analysis across K independently sampled control sets and aggregate the outputs, as noted in Section 2.3. For the fitted spatial field, if $\hat{g}_k(\mathbf{s})$ denotes the surface from bag k , the bagged summary is the pixelwise average

$$\overline{\hat{g}(\mathbf{s})} = \frac{1}{K} \sum_{k=1}^K \hat{g}_k(\mathbf{s}).$$

For the significance maps, let $C_k(\mathbf{s})$ denote the number of Monte Carlo replicate surfaces, out of B , for which $\hat{g}_k^{(b)}(\mathbf{s}) < \hat{g}_k(\mathbf{s})$; $b = 1, \dots, B$. Then the bag-specific exceedance probability is $\hat{p}_{+,k}(\mathbf{s}) = C_k(\mathbf{s})/B$, and the pooled exceedance probability across K bags is

$$\hat{p}_+^{\text{pool}}(\mathbf{s}) = \frac{1}{K} \sum_{k=1}^K \hat{p}_{+,k}(\mathbf{s}) = \frac{\sum_{k=1}^K C_k(\mathbf{s})}{KB}. \quad (12)$$

For the regression coefficients, uncertainty is summarized in two stages. For a single fitted model with estimate $\hat{\boldsymbol{\beta}}$, we compute robust standard errors from the final logistic mean structure with the fitted spatial field treated as a fixed offset. Writing $\hat{p}_i = \text{logit}^{-1}(\mathbf{x}_i^\top \hat{\boldsymbol{\beta}} + \hat{g}(\mathbf{s}_i))$, the covariance estimator is

$$\widehat{\text{Var}}(\hat{\boldsymbol{\beta}}) = (\mathbf{X}^\top \widehat{\mathbf{W}} \mathbf{X})^{-1} \left(\sum_{i=1}^n \hat{r}_i^2 \mathbf{x}_i \mathbf{x}_i^\top \right) (\mathbf{X}^\top \widehat{\mathbf{W}} \mathbf{X})^{-1}, \quad (13)$$

where $\hat{r}_i = y_i - \hat{p}_i$ and $\widehat{\mathbf{W}} = \text{diag}\{\hat{p}_i(1 - \hat{p}_i)\}$. Across the K bags, these coefficient summaries are then combined using a Rubin-style pooling rule. If $\hat{\beta}_{jk}$ denotes the estimate of coefficient j from bag k , and U_{jk} its estimated variance from (13), then the pooled estimate is $\bar{\beta}_j = \frac{1}{K} \sum_{k=1}^K \hat{\beta}_{jk}$, with average within-bag variance $\bar{U}_j = \frac{1}{K} \sum_{k=1}^K U_{jk}$, and between-bag variance $D_j = \frac{1}{K-1} \sum_{k=1}^K (\hat{\beta}_{jk} - \bar{\beta}_j)^2$. The total pooled variance is

$$T_j = \bar{U}_j + \left(1 + \frac{1}{K}\right) D_j, \quad (14)$$

yielding pooled standard error $\sqrt{T_j}$. Wald statistics, confidence intervals, and p-values are then formed from $\bar{\beta}_j$ and T_j , so that the reported coefficient summaries reflect both within-fit uncertainty and the additional variability induced by repeated control sampling.

3.2 Spatio-temporal model

A limitation of the spatial model is that the residual field depends only on geographical position. If the underlying residual risk profile changes over time, then a single fitted surface should be interpreted as a temporally aggregated summary, potentially blending distinct patterns from different periods. When the aim is instead to allow the residual geography to evolve continuously, time must enter the model explicitly.

We therefore consider a spatio-temporal extension in which the residual field depends continuously on event time as well as geographical position. This introduces explicit temporal borrowing, allowing nearby times to contribute to estimation of the residual surface, and avoids the need to partition the study period into prespecified bins (a simpler grouped-time variant is reported in the supplementary materials).

In addition to the previous notation, let $t_i \in \mathbb{R}$ denote the event time for observation i , recorded on a continuous scale. We assume availability of an observation time for controls as well as cases. The model is

$$\text{logit } p_i = \mathbf{x}_i^\top \boldsymbol{\beta} + g(\mathbf{s}_i, t_i), \quad (15)$$

where $g : \mathcal{W} \times \mathbb{R} \rightarrow \mathbb{R}$ is a smooth spatio-temporal residual field, interpreted as the space-time analogue of the residual log-relative-risk surface introduced in Section 3.1. Thus, after adjustment for the fixed-effects component $\mathbf{x}_i^\top \boldsymbol{\beta}$, the function $g(\mathbf{s}, t)$ captures smooth residual departures in event risk over both geography and time. Note that with our year-matched controls, the baseline temporal distribution is already accounted for by design, so a separate global effect of t is not strictly necessary here. Without such matching, one

could augment the linear predictor with an additional term $f(t)$, leaving $g(s, t)$ to represent residual spatio-temporal structure beyond the overall temporal trend.

The general o-IRLS strategy of Section 3.1.2 extends directly to (15), yielding an explicit spatio-temporal residual-risk model within the same orthogonalized framework. This requires moving from a bivariate spatial kernel smoother to a trivariate spatio-temporal one. Several constructions are possible, depending on both the form of the joint kernel and the balance between spatial and temporal smoothing. We adopt a separable Nadaraya-Watson construction, motivated by its continuity with the purely spatial model, its interpretability, and its computational convenience. Closely related forms have been used in standalone spatio-temporal density and relative-risk estimation (e.g. Fernando & Hazelton 2014, Davies et al. 2018, Davies & Lawson 2019).

Specifically, after forming the usual IRLS quantities $\eta_i = \mathbf{x}_i^\top \boldsymbol{\beta} + g(\mathbf{s}_i, t_i)$, $p_i = \text{logit}^{-1}(\eta_i)$, $w_i = p_i(1 - p_i)$, $z_i = \eta_i + \frac{y_i - p_i}{w_i}$, and partial residuals $u_i = z_i - \mathbf{x}_i^\top \boldsymbol{\beta}$, the provisional smooth at a generic space-time point (\mathbf{s}, t) is

$$\tilde{g}(\mathbf{s}, t \mid h, q) = \frac{\sum_{i=1}^n \kappa_h(\|\mathbf{s} - \mathbf{s}_i\|) \tau_q(t - t_i) w_i u_i}{\sum_{i=1}^n \kappa_h(\|\mathbf{s} - \mathbf{s}_i\|) \tau_q(t - t_i) w_i}, \quad (16)$$

where κ_h is the same isotropic spatial kernel used earlier, and τ_q is a one-dimensional temporal kernel with bandwidth q , i.e. $\tau_q(t) = q^{-1}\tau(t/q)$.

Bandwidth selection now entails a joint choice of the pair (h, q) . In principle, the same leave-one-out likelihood cross-validation strategy used in the purely spatial model extends directly to this setting. If $\tilde{g}^{[-i]}(\mathbf{s}_i, t_i \mid h^*, q^*)$ denotes the leave-one-out version of (16) at the i th observed spatio-temporal coordinate under candidate bandwidths (h^*, q^*) , define

$$\eta_{i, \{h^*, q^*\}}^{[-i]} = \mathbf{x}_i^\top \boldsymbol{\beta} + \tilde{g}^{[-i]}(\mathbf{s}_i, t_i \mid h^*, q^*), \quad p_{i, \{h^*, q^*\}}^{[-i]} = \text{logit}^{-1}(\eta_{i, \{h^*, q^*\}}^{[-i]}).$$

The corresponding Bernoulli likelihood CV score is

$$\text{CV}(h^*, q^*) = \sum_{i=1}^n \left[y_i \log p_{i, \{h^*, q^*\}}^{[-i]} + (1 - y_i) \log (1 - p_{i, \{h^*, q^*\}}^{[-i]}) \right], \quad (17)$$

so that the data-driven choice is $(h, q) \leftarrow \arg \max_{h^*, q^*} \text{CV}(h^*, q^*)$.

Relative to the spatial model, however, this optimization is substantially more demanding, since each candidate pair (h^*, q^*) requires repeated leave-one-out smoothing in three dimensions. In addition, the resulting criterion may be relatively flat in one or both directions, making stable joint optimization less straightforward in finite samples. Thus, while (17) is the natural selector in principle, in practice one may instead work over a restricted grid of plausible bandwidth pairs or fix (h, q) in advance on pragmatic grounds.

Rather than producing a single bivariate residual surface, the spatio-temporal model yields a trivariate field describing how residual risk evolves jointly over space and time. In practice, post-fit assessment proceeds by evaluating the fitted field over the study window at a collection of selected time slices t_1^*, \dots, t_m^* . For each such slice, the fitted residual surface $\hat{g}(\mathbf{s}, t^*)$ is mapped over \mathcal{W} , together with its exponentiated form $\exp\{\hat{g}(\mathbf{s}, t^*)\}$.

As in the spatial model, Monte Carlo reassignment is based on repeated refitting under the covariate-only null. For each replicate dataset, this yields a fitted field $\hat{g}^{(b)}(\mathbf{s}, t)$ over space and time. Exceedance-probability maps at any given slice t^* are then formed exactly as in (11), now by comparing the observed and replicated slice-specific surfaces extracted from the full fitted spatio-temporal fields.

With bagging, aggregation is likewise performed after fitting the full spatio-temporal model for each control draw. Let $\hat{g}_k(\mathbf{s}, t^*)$ denote the fitted surface evaluated at time slice t^* for bag k . The bagged summary is the pixelwise average $\overline{\hat{g}(\mathbf{s}, t^*)} = K^{-1} \sum_{k=1}^K \hat{g}_k(\mathbf{s}, t^*)$, while pooled exceedance probabilities are obtained by summing the corresponding slice-specific exceedance counts across bags and dividing by the total number KB of Monte Carlo replicates. Because the fixed-effects component remains common across the full study period, pooling of the regression coefficients and their standard errors is unchanged from the purely spatial model.

4 Results and Interpretation

We now present the results of applying the spatial and spatio-temporal models to the school gun violence data described in Section 2. Throughout, we use a bivariate Gaussian kernel for κ_h and a univariate Gaussian kernel for τ_q . Exceedance probabilities are based on $B = 199$ Monte Carlo replicates, and all results are aggregated over $K = 100$ independently generated control samples.

Convergence of the o-IRLS algorithm is assessed by stabilization of the fitted linear predictor and, where relevant, the regression coefficients. For the purely spatial model, convergence is declared when both the maximum absolute change in β and the maximum absolute change in η between successive iterations fall below 10^{-4} . For the spatio-temporal model, we use a slightly looser criterion based primarily on the linear predictor, declaring convergence when the Fisher-weighted root-mean-square change in η falls below 10^{-3} . This was found to give more stable behavior for the higher-dimensional smoother.

4.1 Parametric component (predictor effects)

A key feature of the present specification is that the regression coefficients are shared across time in the spatio-temporal model, permitting direct comparison with the purely spatial fit. Exploratory analyses suggested curvature in the effects of proportion-white and ADI, so both variables are entered quadratically. Thus, in (1) and (15),

$$\begin{aligned} \mathbf{x}_i^\top \beta \implies & \beta_0 + \beta_1 \text{Enrol}_i + \beta_2 \text{PropMale}_i + \beta_3 \text{Level}[\text{Middle}]_i + \beta_4 \text{Level}[\text{High}]_i + \beta_5 \text{Level}[\text{Other}]_i \\ & + \beta_6 \text{PropWhite}_i + \beta_7 \text{PropWhite}_i^2 + \beta_8 \text{ADI}_i + \beta_9 \text{ADI}_i^2. \end{aligned}$$

Enrollment is log-transformed, ‘Primary/Elementary’ is the reference category for school level, and all numeric predictors are standardized prior to fitting.

Table 1 indicates a clear and stable fixed-effects signal across the spatial and spatio-temporal

fits. The dominant associations are with enrollment and school level: larger schools and, in particular, middle and especially high schools are at materially higher risk than otherwise comparable elementary schools. By contrast, proportion-male contributes little once the remaining predictors are taken into account. The first- and second-order terms for both proportion-white and ADI indicate detectable but more nuanced nonlinear associations, whose shapes are more readily seen in the marginal-effect plots provided in the supplement. Importantly, these school-level effects do not exhaust the structure in the data: they capture compositional differences between schools, but not the broader residual geography examined in Section 4.2.

Parameter	Spatial		Spatio-temporal	
	Est. (S.E.)	p-val.	Est. (S.E.)	p-val.
β_0 (Intercept)	-4.079 (0.121)	< 0.001	-4.053 (0.117)	< 0.001
β_1 (Enrol)	0.860 (0.060)	< 0.001	0.861 (0.060)	< 0.001
β_2 (PropMale)	0.036 (0.061)	0.561	0.045 (0.067)	0.505
β_3 (Level[Middle])	0.559 (0.146)	< 0.001	0.560 (0.145)	< 0.001
β_4 (Level[High])	2.041 (0.105)	< 0.001	2.024 (0.110)	< 0.001
β_5 (Level[Other])	-0.041 (0.378)	0.914	-0.048 (0.379)	0.898
β_6 (PropWhite)	-0.625 (0.073)	< 0.001	-0.608 (0.073)	< 0.001
β_7 (PropWhite ²)	0.177 (0.070)	0.011	0.186 (0.070)	0.008
β_8 (ADI)	0.195 (0.048)	< 0.001	0.194 (0.047)	< 0.001
β_9 (ADI ²)	-0.073 (0.028)	0.009	-0.071 (0.029)	0.015

Table 1: Aggregated parameter estimates, standard errors, and associated Wald test results for the regression coefficients β under the spatial and spatio-temporal fits.

The shapes of the fitted effects for the numeric predictors, particularly the quadratic effects of proportion-white and ADI, are more readily seen in the marginal-effect plots provided in the supplement. As usual, none of the estimated associations should be interpreted causally. This is especially important for those more sensitive variables such as school racial composition or deprivation, which are better viewed as markers of broader structural and historical processes that shape schools and neighborhoods.

The observed stability in β suggests that the main differences between the spatial and spatio-temporal fits will arise in the estimated residual risk surfaces. In other applications, larger discrepancies in β across such models could signal sensitivity of the fixed component to the assumed residual structure, for example because of residual spatial confounding, time-varying covariate effects, or temporal misspecification in the simpler model. Here, however, no such instability is evident.

4.2 Nonparametric component (residual risk)

We now turn to the estimated residual risk surfaces, which are presented graphically. For the spatio-temporal fit, we additionally provide an animation and a three-dimensional iso-surface plot, with interactive versions provided in the supplement and online.

4.2.1 Spatial

For the purely spatial fit, bandwidth selection was carried out using the likelihood cross-validation strategy of Section 3.1.3. Each of the $K = 100$ randomly sampled control sets (“bags”) was accompanied by its own run of the selector. The average selected bandwidth was 159.6 km, with ± 2 standard deviations giving (113.0, 206.3).

The exponentiated pixel-averaged estimate of the residual spatial relative-risk surface, $\exp\{\widehat{g}(\mathbf{s})\}$, is shown in Figure 3. Superimposed are contours of aggregated exceedance probabilities of 0.95 and 0.995, which provide an empirical indication, at two levels, of unusually elevated residual risk.

The dominant feature of Figure 3 is a broad corridor of elevated residual risk extending through the central and eastern United States. The strongest contiguous exceedance contours run through parts of the lower Midwest and Ohio Valley, across Kentucky and Tennessee, and into the central Appalachian region. This indicates that, even after adjust-

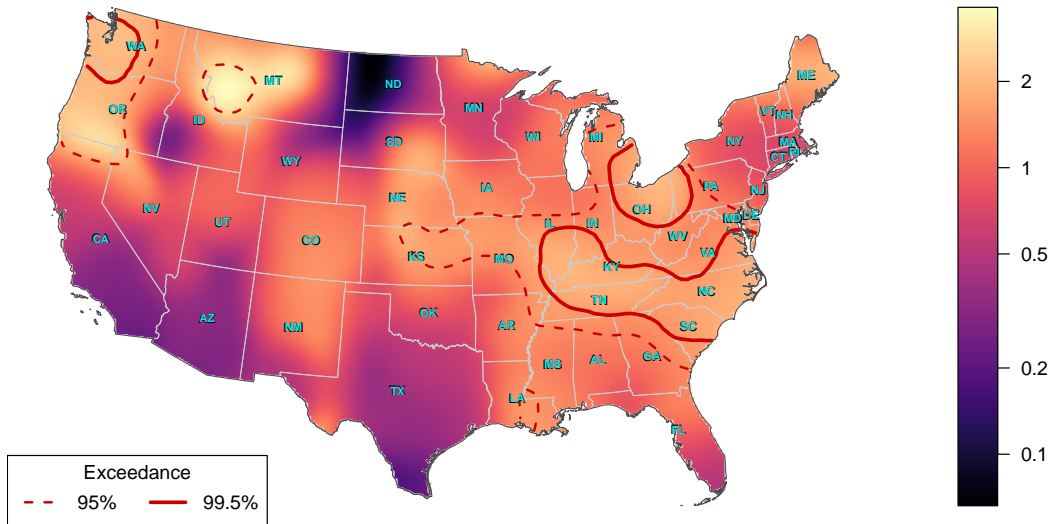


Figure 3: Estimated residual relative risk surface for the purely spatial fit. Log color scale.

ment for the observed school-level covariates, the incidence of school gun violence events remains systematically higher in this corridor than would be expected from the background distribution of schools alone. By contrast, much of the far West and parts of the southern border region exhibit comparatively attenuated residual risk, with values of $\exp\{\overline{\hat{g}}(\mathbf{s})\}$ below unity over substantial areas and little corresponding exceedance evidence. This is especially noticeable across California, Arizona, and parts of Texas. This pattern should not be read simply as a consequence of sparse school coverage. Because the controls are drawn from the background school population, the comparison remains relative to the local distribution of schools. Across much of the West, the fitted residual risk is generally near or below the covariate-adjusted background level rather than unusually elevated.

Smaller but still coherent localized pockets of elevated residual risk are also present, most visibly in the far Northwest, the northern Rocky Mountain region, and around parts of the Great Lakes. Taken together, the spatial fit shows that the remaining unexplained risk of school gun violence incidents is not diffuse, but organized into several geographically coherent zones, the most prominent of which lies in the central-eastern half of the country.

As a diagnostic, we also compared these orthogonalized spatial fits with a non-orthogonalized

backfitting version (Kelsall & Diggle 1998) using the same fixed bandwidth within each control draw. The results were compelling. Across the 100 bags, the unorthogonalized smooth consistently exhibited substantial overlap with the weighted fixed-effects space and produced systematic shifts in several regression coefficients. The broad residual geography remained similar, but the difference between the two fits was nevertheless nontrivial and spatially structured, indicating a broad reallocation of the smooth component when orthogonalization was removed. This supports the practical role of orthogonalization in preserving the interpretation of the smooth term as genuinely residual risk; full details of this comparison are provided in the supplementary document.

4.2.2 Spatio-temporal

We turn now to the spatio-temporal fit. As noted in Section 3.2, automatic bandwidth selection for the full trivariate smoother is practically demanding. For the present analysis, we therefore work with fixed bandwidths chosen from exploratory runs and guided in part by the maximal smoothing principle (Terrell 1990) applied separately to the spatial and temporal margins. The spatial bandwidth was set at 230 km and the temporal bandwidth at $q = 578$ days (≈ 1.5 years). Sensitivity checks using nearby bandwidth settings ($\times 0.75$ and $\times 1.5$) did not materially alter the main conclusions: smaller bandwidths yielded a more granular estimated field and larger bandwidths a smoother one, but the dominant eastern residual-risk regime and the fixed-effects conclusions remained stable.

The continuous-time bagged estimate $\exp\{\overline{\hat{g}(\mathbf{s}, t)}\}$ is most naturally viewed as an animation. This is provided in the supplement and at <https://www.stats.otago.ac.nz/research/davies-gv/animation.mp4>. We also construct a trivariate contour display with translucent iso-surfaces representing the same elevated exceedance probabilities; an interactive version is likewise provided in the supplement and at <https://www.stats.otago.ac.nz/research/davies-gv/exceed.html>.

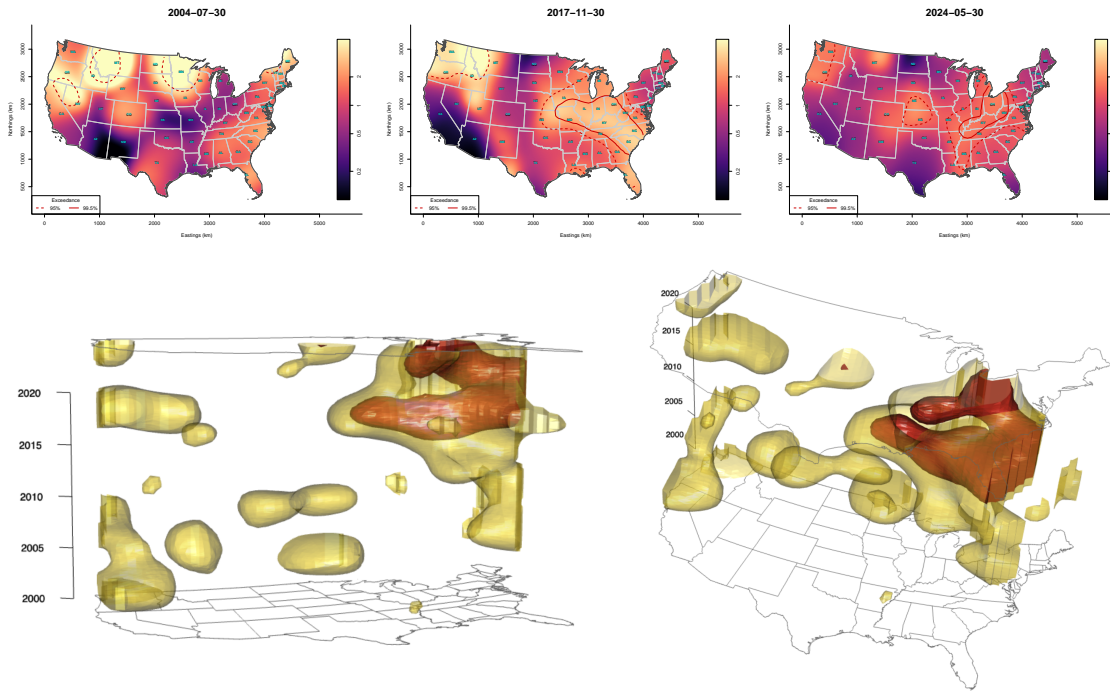


Figure 4: Stills of the bagged spatio-temporal odds ratio $\exp \overline{\hat{g}(\mathbf{s}, t)}$ and accompanying exceedance contours: three selected frames from the animation (top row) and two viewing angles of the trivariate iso-surfaces of high exceedance probabilities (bottom row).

Viewed as a full space-time object, the exceedance structure reveals more than the standalone spatial map. The dominant feature is a connected central-eastern region of elevated residual risk, with the 95% exceedance surface spanning a broad volume through parts of the Midwest, Appalachia, and the Southeast, and the 99.5% surface embedded within it as a more concentrated core. This indicates not merely repeated appearance of elevated risk in successive periods, but a comparatively persistent space-time regime of excess residual risk. That concentrated core is most evident in the later part of the study period. Thus, after adjustment for both the school-level predictors and the background distribution of schools, the strongest residual elevation in school gun violence risk appears in the eastern half of the country, especially in the more recent years. In particular, the strongest recent coverage of high exceedance probabilities runs through parts of Missouri, Kentucky, Tennessee, Illinois, Indiana, Ohio, Virginia, West Virginia, and the Carolinas, with broader elevated structure

extending into parts of the Southeast.

Outside this dominant eastern regime, western and interior features generally appear as smaller detached bodies in space-time, suggesting more localized and often more episodic periods of elevated residual risk. Some western features, particularly in the Pacific Northwest, also appear to recur across multiple periods rather than representing purely isolated spikes. In this sense, the spatio-temporal fit sharpens the interpretation of the purely spatial surface: the residual geography is not only time-varying, but dominated by a persistent eastern corridor whose intensity strengthens in later years, alongside a collection of smaller regional features that vary in timing and duration.

5 Concluding Remarks

This paper develops a covariate-adjusted framework for residual risk mapping in case-control event data and extends it from the purely spatial setting to explicit spatio-temporal analysis. By orthogonalizing the smooth component against the fixed effects, the approach separates explained variation from residual geographic and temporal concentration while retaining an interpretable kernel-based representation of excess risk.

Applied to gun violence incidents at K-12 schools, the analysis yields a clear empirical picture. The fixed-effects results are stable across the spatial and spatio-temporal fits: larger schools and secondary schools are at markedly higher risk, while the remaining school-level covariates play a more modest role once the full model structure is taken into account. More importantly, the residual component reveals that the remaining excess risk is not incidental or spatially diffuse, but concentrated in a persistent central-eastern corridor after adjustment for both school-level covariates and the background distribution of schools. In this sense, the analysis suggests that nationwide school gun violence risk is structured not only by school composition, but also by broader contextual forces that remain spatially

organized even after those school-level characteristics have been accounted for.

Substantively, these findings point to a natural next step: more targeted regional or state-level follow-up analyses aimed at understanding the drivers of elevated residual risk, particularly in locations where that risk appears strongest and most persistent in recent periods. For example, such analyses could help connect the residual risk surface to broader contextual factors such as firearm policy, law enforcement presence, or underlying economic conditions at the community level. Of particular note is the post-2017 intensification of this corridor, which suggests a recent shift in underlying conditions not captured by school characteristics alone. This temporal pattern is suggestively consistent with emerging state-level evidence that firearm-law environments are associated with school-shooting incidence (Wippell et al. 2026), though the present analysis does not attribute the observed residual structure to any single policy mechanism.

More generally, our results illustrate the value of treating residual risk surfaces as inferential objects in their own right rather than as nuisance terms attached to the linear predictor. The broadly applicable framework developed here therefore offers a practical and interpretable extension of kernel-based case-control regression that cleanly separates fixed effects from spatio-temporally evolving residual risk.

6 Disclosure statement

The authors report there are no competing interests to declare.

7 Data Availability Statement

The authors confirm that the data supporting the findings of this study are available within the article and its supplementary materials.

SUPPLEMENTARY MATERIAL

Additional Details: A document providing additional definitions, diagnostic comparisons, and other results signaled in the text. (`SupplementAdditionalDetails.pdf`)

Data and Code: R scripts and data files needed to fully replicate results. (`data_and_code.zip`)

Pre-stored Results: R objects giving pre-stored results; spatio-temporal animation/widget objects. (`result_objects.zip`)

References

- Bader, M. D. M. (2025), ‘Spatial analysis of the social world’, *Annual Review of Sociology* **51**, 129–147.
- Bithell, J. F. (1991), ‘Estimation of relative risk functions’, *Statistics in Medicine* **10**(11), 1745–1751.
- Comer, B. P. (2024), ‘Definitional discrepancies: Defining “school shootings” and other incidents of gunfire affecting schools’, *Social Sciences* **13**(6), 316.
- Davies, T. M. & Lawson, A. B. (2019), ‘An evaluation of likelihood-based bandwidth selectors for spatial and spatiotemporal kernel estimates’, *Journal of Statistical Computation and Simulation* **89**(7), 1131–1152.
- Davies, T. M., Marshall, J. C. & Hazelton, M. L. (2018), ‘Tutorial on kernel estimation of continuous spatial and spatiotemporal relative risk’, *Statistics in Medicine* **37**, 1191–1221.
- Fernando, W. T. P. S. & Hazelton, M. L. (2014), ‘Generalizing the spatial relative risk function’, *Spatial and Spatio-temporal Epidemiology* **8**, 1–10.
- Fridel, E. E. (2021), ‘The contextual correlates of school shootings’, *Justice Quarterly* **38**(4), 596–625.

- Gammell, S. P., Connell, N. M. & Huskey, M. G. (2022), ‘A descriptive analysis of the characteristics of school shootings across five decades’, *American Journal of Criminal Justice* **47**(5), 818–835.
- Gatrell, A. C., Bailey, T. C., Diggle, P. J. & Rowlingson, B. S. (1996), ‘Spatial point pattern analysis and its application in geographical epidemiology’, *Transactions of the Institute of British Geographers* **21**(1), 256–274.
- González, J. A., Rodríguez-Cortés, F. J., Cronie, O. & Mateu, J. (2016), ‘Spatio-temporal point process statistics: A review’, *Spatial Statistics* **18**, 505–544.
- Hodges, J. S. & Reich, B. J. (2010), ‘Adding spatially-correlated errors can mess up the fixed effect you love’, *The American Statistician* **64**(4), 325–334.
- Joseph, J. J. & Purser, C. W. (2023), ‘An examination of the role of perpetrator’s relationship to overall school shooting casualties’, *Laws* **12**(4), 73.
- Kelsall, J. E. & Diggle, P. J. (1995), ‘Kernel estimation of relative risk’, *Bernoulli* **1**, 3–16.
- Kelsall, J. E. & Diggle, P. J. (1998), ‘Spatial variation in risk of disease: A nonparametric binary regression approach’, *Journal of the Royal Statistical Society: Series C (Applied Statistics)* **47**(4), 559–573.
- Kolbe, L. J. (2020), ‘School gun violence in the United States’, *Journal of School Health* **90**(3), 245–253.
- Nowicki, J. M. (2020), K-12 education: Characteristics of school shootings, Technical Report GAO-20-455, United States Government Accountability Office, Washington DC.
- Richardson, E. G. & Hemenway, D. (2011), ‘Homicide, suicide, and unintentional firearm fatality: Comparing the United States with other high-income countries, 2003’, *The Journal of Trauma* **70**(1), 238–243.

- Riedman, D. (2025), ‘K-12 School Shooting Database’, <https://k12ssdb.org/>.
- Rowhani-Rahbar, A. & Moe, C. (2019), ‘School shootings in the U.S.: What is the state of evidence?’, *Journal of Adolescent Health* **64**(6), 683–684.
- Stewart, I., Wertz, J. & Jen, H. (2022), ‘School-associated violent deaths in the United States: A comprehensive review of the literature’, *Journal of School Violence* **21**(4), 450–475.
- Terrell, G. R. (1990), ‘The maximal smoothing principle in density estimation’, *Journal of the American Statistical Association* **85**(410), 470–477.
- Velázquez, E., Martínez, I., Getzin, S., Moloney, K. A. & Wiegand, T. (2016), ‘An evaluation of the state of spatial point pattern analysis in ecology’, *Ecography* **39**(11), 1042–1055.
- Wippell, J. G. R., Haynie, D. L. & Riedman, D. (2026), ‘Preventable tragedies: A longitudinal analysis of state firearm laws and K-12 school shootings in the United States (2000–2019)’, *Social Science & Medicine* **394**, 119049.
- Wood, S. N. (2017), *Generalized Additive Models: An Introduction with R*, 2 edn, Chapman and Hall/CRC, Boca Raton.